Received: 7 July 2021 | Revised: 12 January 2022 | Accepted: 2 May 2022

DOI: 10.1002/pip.3578

SPECIAL ISSUE ARTICLE

PROGRESS IN PHOTOVOLTAICS WILEY

Failure diagnosis and trend-based performance losses routines for the detection and classification of incidents in large-scale photovoltaic systems

Andreas Livera[1] | Marios Theristis[2] | Leonardo Micheli[3] | Joshua S. Stein[2] | George E. Georghiou[1]

[1]PV Technology Laboratory, FOSS Research Centre for Sustainable Energy, Department of Electrical and Computer Engineering, University of Cyprus, Nicosia, Cyprus

[2]Sandia National Laboratories, Albuquerque, NM, USA

[3]Advances in Photovoltaic Technology (AdPVTech), CEACTEMA, University of Jaén, Jaén, Spain

Correspondence
Andreas Livera, PV Technology Laboratory, FOSS Research Centre for Sustainable Energy, Department of Electrical and Computer Engineering, University of Cyprus, Nicosia 1678, Cyprus.
Email: livera.andreas@ucy.ac.cy

Present address
Leonardo Micheli, Department of Astronautical, Electrical and Energy Engineering (DIAEE), Sapienza University of Rome, Rome, Italy.

Funding information
U.S. Department of Energy's Office of Energy Efficiency and Renewable Energy (EERE), Grant/Award Number: 38267; European Commission within the EU Framework Programme for Research and Innovation HORIZON 2020, Grant/Award Number: 691664; Research and Innovation Foundation (RIF) of Cyprus; Ministry of Economy, Industry and Competitiveness—State Research Agency (MINECO-AEI); General Secretariat for Research and Technology (GSRT)

Abstract

Fault detection and classification in photovoltaic (PV) systems through real-time monitoring is a fundamental task that ensures quality of operation and significantly improves the performance and reliability of operating systems. Different statistical and comparative approaches have already been proposed in the literature for fault detection; however, accurate classification of fault and loss incidents based on PV performance time series remains a key challenge. Failure diagnosis and trend-based performance loss routines were developed in this work for detecting PV underperformance and accurately identifying the different fault types and loss mechanisms. The proposed routines focus mainly on the differentiation of failures (e.g., inverter faults) from irreversible (e.g., degradation) and reversible (e.g., snow and soiling) performance loss factors based on statistical analysis. The proposed routines were benchmarked using historical inverter data obtained from a 1.8 MWp PV power plant. The results demonstrated the effectiveness of the routines for detecting failures and loss mechanisms and the capability of the pipeline for distinguishing underperformance issues using anomaly detection and change-point (CP) models. Finally, a CP model was used to extract significant changes in time series data, to detect soiling and cleaning events and to estimate both the performance loss and degradation rates of fielded PV systems.

KEYWORDS
anomaly detection, change-point detection, data analytics, failure diagnosis, monitoring, performance loss, photovoltaics

1 | INTRODUCTION

As photovoltaic (PV) systems are rapidly becoming an important part of the energy mix, it is important to ensure their reliability and maximize their energy output to reduce the levelized cost of electricity (LCoE). This can be achieved through advanced data analytics.[1]

To reliably generate electricity during an extended lifetime, cutting-edge software and data-driven algorithms can be employed to

monitor the PV plant health state and detect real-time failures, thus minimizing downtimes. This will increase the energy yield and the profitability of the system.[2]

Currently, most of the utility-scale PV power plants around the world are monitored 24/7, generating high volumes of data. Depending on the level of monitoring, the analysis of field data can indicate different failures and/or loss mechanisms and it can provide insights on corrective, preventive, and predictive maintenance.[3] However, to optimize the operation and maintenance (O&M) strategies and maximize revenues, PV plant owners and asset managers must rely on efficient ways for analyzing and interpreting the data streams. By doing this, fault incidents can be detected early and classified into different fault categories, thus enabling operators to take appropriate actions to mitigate the losses.[2,4]

Typical automated failure detection can be categorized as: model-based, image and data-driven methods.[5–19] Such implementations mainly utilize electrical and meteorological measurements, signals, or images to capture the behavior of PV systems, uncover patterns, and identify failures. Most of the failure detection methods define threshold levels (TLs), which are used to compare a PV performance model against measurements in order to identify fault conditions.[20–24] Other methodologies perform residual analysis and statistical tests to detect faults in PV systems.[22–29] Even though some commonly occurring PV failures can be detected by the proposed algorithms, the categorization of incidents into different failure types and loss mechanisms remains a challenging task.[30]

Although several machine learning-based models have been reported in the literature,[10,13,31–39] it is unknown if any are indeed used (or even applicable) for real-time or post-processing monitoring applications, at the moment. On the other hand, the industry has been applying numerous statistical, empirical, and physics-based approaches to analyze the health state or performance losses of PV power plants. For example, python libraries have been developed to simulate PV performance (e.g., *pvlib-python*[40]) or to evaluate PV performance based on statistical time series analysis (e.g., *RdTools*[41,42]). In *pvlib-python*, it is possible to estimate the fraction of DC power lost due to snow coverage, soiling and shading. However, besides the site's meteorological measurements, other assumptions and parameters are required, which might not be readily available (e.g., particulate matter data, number of strings per module, and tilt). Similarly, the *RdTools* open-source library has the capability of statistically obtaining rates of performance degradation and soiling loss, which are useful for overall health state assessment. However, *RdTools* does not differentiate the performance loss rate (PLR) from the degradation rate (R_D). Though, a new capability was added for extracting simultaneously soiling losses and PLR.[43] Other existing methods rely on *I–V* curves and weather data and require train and test datasets for failure classification based on the exhibited profiles and fault patterns.[33,36] *I–V* data, PV module/string level measurements, and labeled datasets are not usually available in real PV installations making most of the proposed failure classification methodologies not universally applicable in large-scale PV systems.

Current best practices lack a methodology for the accurate differentiation of failures and reversible/irreversible performance losses. Reversible and irreversible performance losses are referred to as "trend-based" performance losses as their effect is either gradual or seasonal rather than failure-based losses that occur in an instant, and therefore, can be detected and quantified based on time series analysis. Differentiating and quantifying individual trend-based performance losses in real field data is a challenging task due to the complex interactions of PV behavior with changing environmental conditions as well as measurement noise, erroneous data, and uncertainties. To address this gap, failure diagnosis routines (FDRs) and trend-based performance loss routines (TLRs) were developed based on statistical residual[25,44] and change-point (CP)[45] techniques. The proposed routines operate on PV operational data and meteorological measurements and complement the previously developed data quality routines (DQRs).[4] All routines were combined to derive a complete diagnostic pipeline for differentiating common PV failures and performance losses (such as zero and reduced power production, degradation, soiling and snow losses) from a single performance metric. The diagnostic pipeline can be used for batch time series analyses of large fleets and real-time monitoring given that the technical specifications of the PV systems are available (e.g., system characteristics and meteorological data). The pipeline was benchmarked experimentally using historical inverter level measurements from a PV power plant in Larissa, Greece.

2 | METHODOLOGY

The proposed routines operate on time series of meteorological and electrical measurements. DQRs are initially applied for data validation and filtering of outliers, while power simulation models are used for predicting the performance of the system in the absence of any failures or degradation. FDRs are then used for detecting and classifying failures, while TLRs are utilized for detecting performance losses. Statistical analysis is then performed to distinguish faults from reversible and irreversible mechanisms. The proposed methodology, illustrated in Figure 1, was validated using the maintenance logs.

2.1 | DQRs

Initially, the methodology for data processing and quality verification was applied to the PV dataset to identify and remove invalid data points before simulating the plant performance. This can also provide insights and information about possible failures/performance losses and their type (e.g., near zero power production incidents).[2] More details about the DQR process are available in Livera et al.[4]

2.2 | PV system performance models

The Huld et al.[46] model was used to predict the DC power of the test PV system. The model requires the in-plane irradiance and module

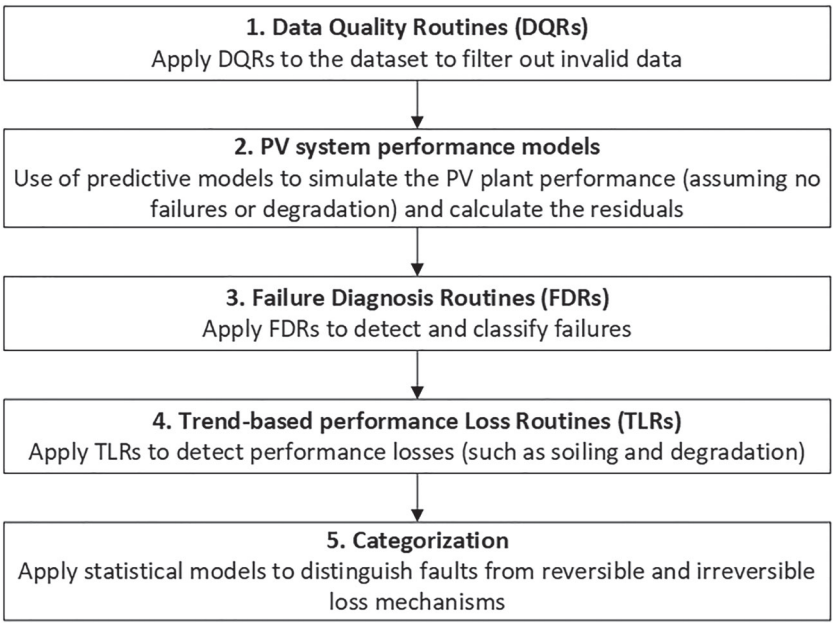

FIGURE 1 Flowchart of the proposed methodology describing the five consecutive steps for differentiating failures and trend-based performance losses

temperature measurements. It was selected due to its high accuracy for c-Si PV modules under different sky conditions (e.g., clear-sky, cloudy, and partly cloudy conditions).[47] For the DC current and voltage measurements predictions, the empirical parametric models described by Livera et al.[33] were used.

The simulation models for predicting the power, current, and voltage measurements were trained based on a 10%:90% train and test set approach. The train set contained fault-free data over a 6-month period, and it was used for the model's training process—deriving the model's coefficients. The rest of the dataset, 54 months of data containing both faulted and fault-free periods, was used for the testing process. The goodness of the models' fit was evaluated using the correlation coefficient (R), the coefficient of determination (R^2), the mean absolute percentage error (MAPE), and the root mean square error (RMSE).[48] The Huld et al. model[46] was then used as a reference model in the failure diagnostic procedure by performing comparisons between the actual/measured and predicted/simulated power.

The performance ratio (PR), power, current, and voltage residuals, defined as the difference between the predicted and measured values, were also calculated.

2.3 | FDRs

The developed FDRs include a failure detection and a classification stage. The detection stage is based on a comparative assessment between the predicted and measured DC energy yield. A failure is detected when the absolute error (AE), defined as the absolute difference between the predicted and measured DC power, exceeds a specified TL. The TL is calculated by multiplying the power of the array at Standard Test Conditions (STC) with the combined yield uncertainty of the performance model. The combined uncertainty is calculated by deriving the partial derivatives of the model's inputs.[49]

Residual analysis was performed to verify the fault occurrences. In this context, the power, current, and voltage residuals from the seasonal naive method were analyzed using Shewhart charts (also known as control charts).[26,50] In a Shewhart chart, a sequence of samples is plotted against time and upper and lower control limits (UCL and LCL) are calculated based on the three-sigma rule; that is, UCL, LCL $= \mu_0 \pm 3\sigma_0$, where μ_0 is the process mean and σ_0 is the standard deviation.[25] The UCL and LCL were calculated over weekly sliding windows using data under normal operation.[25] Under normal operation, the residuals are close to zero, have constant variance, and are normally distributed and within the estimated limits. During fault conditions, the residuals significantly deviate from zero and exceed the estimated control limits.

Once fault conditions are identified, classification algorithms based on logic tree structures[33] are used to categorize the detected incidents into (a) near zero power production (0% to 15% of predicted power due to inverter shutdown failures, grid problems, ground faults, etc.) and (b) nonzero production (due to snow coverage, degradation, soiling, etc.).[51] Nonzero production incidents due to failures were further categorized into three groups: (a) reduced current production class, (b) reduced voltage production class, and (c) reduced current–voltage production class. More details are given in Section 2.5 and Table 1.

2.4 | TLRs

Trend-based performance losses refer to linear and nonlinear drops in performance time series and profiles that may reduce the produced power of a PV system by up to 20%.[56] However, in some cases such as heavy snowfall or sandstorm, this range can be exceeded.[54] Such phenomena are categorized as nonzero production incidents and they can result in reversible and irreversible performance losses based on

TABLE 1 Summary of the different fault and loss profiles that were investigated in this study

Fault/loss type	Power reduction (%) compared with predicted power	Required electrical and weather parameters	Anomalies and change-point (CP) detection	Residual pattern and rate changes	Exhibited profile
Near zero production	85–100	G_I, T_{mod}[a]/T_{amb}, P_{DC}, I_{DC}	Data anomalies	High deviation from zero	Reduced P_{DC}
Nonzero production due to faults (current–voltage class)	20–85	G_I, T_{mod}[a]/T_{amb}, P_{DC}, I_{Dc}, V_{DC}	Data anomalies	High deviation from zero with sudden changes (anomalies) in power, current, and voltage residuals	Reduced P_{DC}, I_{Dc}, V_{DC}
Nonzero production due to faults (current class)	20–85	G_I, T_{mod}[a]/T_{amb}, P_{DC}, I_{DC}	Data anomalies	High deviation from zero with sudden changes (anomalies) in power and current residuals	Reduced P_{DC}, I_{DC}
Nonzero production due to faults (voltage class)	20–85	G_I, T_{mod}[a]/T_{amb}, P_{DC}, V_{DC}	Data anomalies	High deviation from zero with sudden changes (anomalies) in power and voltage residuals	Reduced P_{DC}, V_{DC}
Nonzero production due to loss incidents - Soiling	Up to 20[b]	G_I, T_{mod}[a]/T_{amb}, rainfall and wind data, P_{DC}, I_{Dc}	CP anomalies Continuous CPs	Low deviation from zero during time periods with no rainfall and between cleaning events (discontinuous CPs—positive shifts). Negative rate changes	Reduced P_{DC}, I_{DC}
Nonzero production due to loss incidents - Snow coverage	Up to 20[b]	G_I, T_{mod}[a]/T_{amb}, snowfall data, P_{DC}, I_{DC}, V_{DC}	CP anomalies Continuous CPs	Low deviation from zero during snowfall time periods. Negative rate changes	Reduced P_{DC}, I_{DC}, V_{DC} "Low" T_{amb}
Nonzero production due to loss incidents - Degradation	Up to 20[b]	G_I, T_{mod}[a]/T_{amb}, P_{DC}, I_{DC}	CP anomalies Continuous CPs	Decreasing trend over years—progressive power drop	Reduced P_{DC} and I_{DC} (V_{DC} may also be affected)

Abbreviations: G_I, in-plane irradiance; I_{DC}, DC current; P_{DC}, DC power; T_{amb}, ambient air temperature; T_{mod}, module temperature; V_{DC}, DC voltage.
[a]Module temperature measurements can be simulated using an empirical model (i.e., using the Sandia module temperature model,[52] the Ross thermal model,[53] or the open-source Faiman module temperature available in *pvlib-python* library[40]).
[b]In some specific cases (e.g., heavy snowfall or sandstorm, severe potential-induced degradation), trend-based performance losses can cause power reductions greater than 20%.[54,55]

the caused damage.[57] Most of the irreversible losses can be classified as material/component degradation of the PV module and balance of system.[57]

In this study, degradation, soiling, and snow coverage were investigated by applying a statistical method on a single PV performance metric. A statistical CP algorithm was utilized to identify the number and location(s) of CP(s) in a given profile by capturing linear and complex trends as well as abrupt profile changes.[58–60] A change- or switch- or break-point refers to a change in a time series or trend's statistical properties (e.g., mean, variance, and slope).[58] A time series with m CPs splits the data into $m + 1$ segments. The detected changes can be continuous or discontinuous. In the case of performance losses, continuous CPs indicate a variation in the rate at which soiling accumulates or a nonlinear degradation pattern.[60] In case of nonlinear degradation, changes in the variability of PR time series are detected with the different segments exhibiting different slopes.[61] On the other hand, discontinuous CPs can either indicate soiling cleaning events, snow shedding, or corrective maintenance actions.[60]

The TLRs consist of the Facebook Prophet (FBP)[59] CP algorithm for estimating either the linear or nonlinear PLR from the PR time series. FBP is an open-source library, available in Python and R, used to forecast time series based on an additive decomposition model, which combines trend, seasonality, and holidays (neglected in this paper).[62] A piecewise linear model is applied by default for the trend, whereas the seasonal model is similar to the exponential smoothing in the Holt–Winters[63] technique. The FBP model was selected due to its ability to decompose the signal, perform CP

analysis, and adjust the trend flexibility and its additional functionalities (e.g., forecasting).[58] This model was also applied to PV performance time series and exhibited low prediction error under different conditions (e.g., two- and three-step degradation profiles, range of PV module technologies seasonality in different climate zones, and different aggregation).[64]

The FBP algorithm detects the number and location(s) of CPs by capturing statistical changes in the slopes of predefined segments. It initially distributes "potential" CPs uniformly along the selected range of the time series' trend, and it then compares the slopes in order to extract the most significant CPs by performing comparisons against a set TL.[58,59] The FBP algorithm calibration procedure was performed as reported by Theristis et al.[58]

In this work, 100 "potential" CPs were distributed on the PR time series (*n_changepoints* = 100) and the *changepoint_range* argument was set to 1 because the analysis does not project trends into the future. The flexibility (*changepoint_prior_scale* argument), however, needs to be adjusted depending on the application and the utilized performance metric. Initially, the *changepoint_prior_scale* was set to 2.5[65] to extract PLR, which includes both reversible and irreversible performance losses. The *changepoint_prior_scale* argument can then be adjusted to control the fluctuations. For example, if the value is decreased (e.g., 0.04),[64] an almost linear trend will be forced, which avoids fluctuations due to outliers (e.g., faults), or other temporary effects such as snow and soiling. In this case, the FBP model will be extracting rates of irreversible effects caused by linear/nonlinear degradation. On the other hand, if the *changepoint_prior_scale* value is increased, it will result in a fluctuating trend that will be able to capture temporary phenomena. However, this needs to be calibrated according to Theristis et al.[58] because if the *changepoint_prior_scale* is set too high, it will result in a highly fluctuating trend, which might even capture unavoidable seasonality effects caused by irradiance, temperature, spectrum, and so on. Therefore, based on the *changepoint_prior_scale* setting, the different CPs and their sequence (i.e., continuous or discontinuous) will represent different events and types of performance loss.

For the case of soiling, the PR residuals were examined for continuous and discontinuous CPs in the time series by setting the *changepoint_prior_scale* argument to 1.4.[60] Continuous CPs indicate a change in the daily variation of the soiling loss, in %/year, also called soiling rate. The soiling rate can be estimated during the deposition periods as the slope of the PR between the cleaning events, by applying linear regression.[66] Discontinuous CPs indicate cleaning events caused by either artificial or natural cleaning. Artificial and natural cleaning events cause positive shifts in the running median of the investigated time series and the time between two consecutive cleanings is called the "deposition period." The scope of the devised CP model is to determine when the soiling deposition trend changes and consequently estimate the soiling loss.

Snow exhibits similar time series patterns as soiling, and therefore, additional information from meteorological data is required to automatically differentiate these loss mechanisms (more details in Section 2.5).

2.5 | Categorization

Categorization of nonzero power production incidents was performed using a single PV performance metric.

The Seasonal Hybrid Extreme Studentized Deviates (S-H-ESD) was initially applied to detect data anomalies in the PR time series.[67,68] Data anomalies cause sudden increase or decrease in time series data and indicate fault occurrences and data issues. The S-H-ESD anomaly detection algorithm is an extension of the generalized Extreme Studentized Deviates (ESD).[69] In the ESD algorithm, sample mean and standard deviation are used for identifying anomalies in a given time series, while the S-H-ESD model uses the median for minimizing the number of false positives (FPs) detected by the model. The S-H-ESD model was selected due to its ability to detect both global and local anomalies by applying Seasonal and Trend decomposition using Loess[27] and robust statistics (i.e., statistical test hypothesis, median based estimation, and piecewise approximation) together with ESD.[69]

The FBP algorithm was used to detect CPs, differentiate reversible from irreversible mechanisms and to estimate the PLR and R_D.[59] Initially, PLR is extracted with a *changepoint_prior_scale* setting of 2.5 to assess the overall health state of the plant. The rates of change for each slope are then compared against a set TL to verify the CPs and detect reversible mechanisms. These loss mechanisms are then differentiated based on the magnitudes of the rates of change and the distance between these CPs. However, both soiling and snow might exhibit similar behavior in weather-agnostic PR time series. For example, a negative rate of change switching to positive within a week can indicate weather dependent phenomena such as snow accumulation and shedding or a sandstorm followed by rain. In this case, the categorization procedure uses information from weather parameters to enable differentiation of snow and soiling. During snowfall periods, the PV system power production is reduced, while the module and ambient temperature measurements are lower than the typical operating temperature ranges. It is worth noting here that this is a seasonally repeated performance loss that affects all three electrical parameters (current, voltage and hence power).[70] Additionally, when snow sheds, an increase in the recorded voltage measurements is initially observed followed by a stepwise reduction.[70]

The *changepoint_prior_scale* setting of FBP is then readjusted to estimate R_D and to detect soiling and cleaning events. All quantitative metrics, specifications, and models used for differentiating fault types from loss mechanisms in PV systems are summarized in Figure 2 and Table 1 (presented in Section 2.3).

2.6 | Benchmarking and validation

The diagnostic architecture was benchmarked using time series data from a 1.8 MWp PV power plant in Larissa, Greece (Köppen–Geiger–Photovoltaic climate classification DH; temperate with high irradiation).[71] The crystalline silicon (c-Si) PV modules are facing south, fixed-tilted at 25°, and they are connected in series to form 326 strings

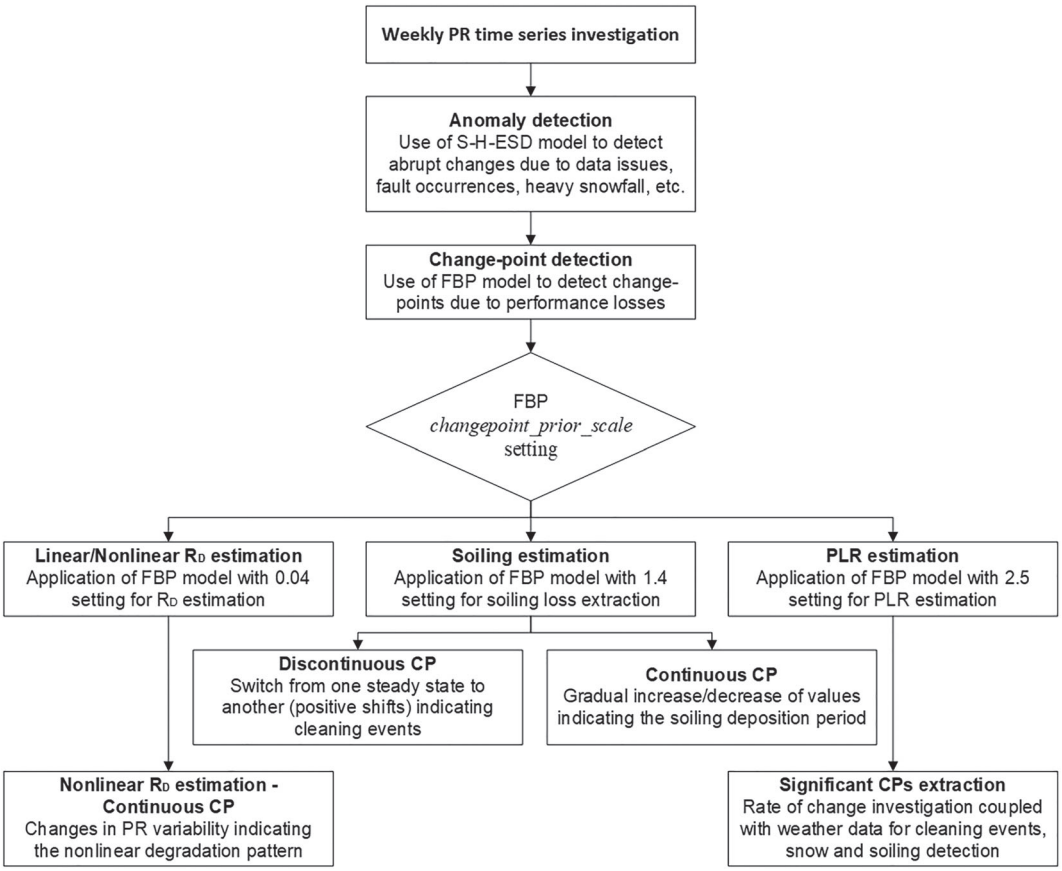

FIGURE 2 Investigation of the performance ratio (PR) time series for differentiating fault types from loss mechanisms using statistical analysis. Data anomalies and change-points (CPs) are detected using the Seasonal Hybrid Extreme Studentized Deviates (S-H-ESD) and Facebook Prophet (FBP) models, respectively. Data anomalies indicate data issues and fault occurrences, while CP anomalies indicate performance losses and cleaning/repair actions, captured by adjusting the FBP's flexibility (*changepoint_prior_scale* hyperparameter)

at the inputs of four grid-connected inverters (82 strings are connected to Inverters 1 and 3, while 81 strings are connected to Inverters 2 and 4) and four transformers.

The PV plant is connected to a data acquisition (DAQ) system, which is used for the monitoring and storage of meteorological and inverter data according to the requirements set by the IEC 61724-1.[72] The DAQ records values of in-plane irradiance (G_I), ambient air temperature (T_{amb}), wind speed, and direction. The PV operational data include the back-surface module temperature (T_{mod}), the inverter DC current (I_{DC}), voltage (V_{DC}) and power (P_{DC}), and AC output power (P_{AC}) at a resolution of 1 s and accumulation steps of 15-min averages. Yields and performance parameters such as the PV array energy yield (Y_A), the final PV system yield (Y_f), the reference yield (Y_r), and the DC PR were also calculated.[73] Lastly, weather data that were unavailable at the power plant (e.g., snowfall and rainfall measurements) were sourced from Modern-Era Retrospective analysis for Research and Applications, Version 2 (MERRA-2).[74] These were downloaded at hourly intervals through the soda-pro web interface.

The outdoor field measurements and the calculated performance metrics were used to create a PV dataset of 15-min average measurements from the four grid-connected inverters from June 1, 2013, to December 31, 2018. Over the evaluation period, the PV plant experienced different underperformance issues (i.e., plant was down due to grid failures, scheduled maintenance, inverter and ground faults, low power production and/or low performance due to snowfall, equipment malfunctions, and soiling). Information about the outage periods, failure types, loss mechanisms, and corrective actions were kept in a maintenance log, which was then used for validating the performance of the diagnostic algorithms.

TABLE 2 2×2 confusion matrix for evaluating the performance of the failure diagnosis routines

	Predicted normal operation data points	Predicted fault data points
Actual normal operation data points	TP	FN
Actual fault data points	FP	TN

In order to evaluate the detection and classification accuracy of the FDRs, a 2×2 confusion matrix (see Table 2) was used.[75]

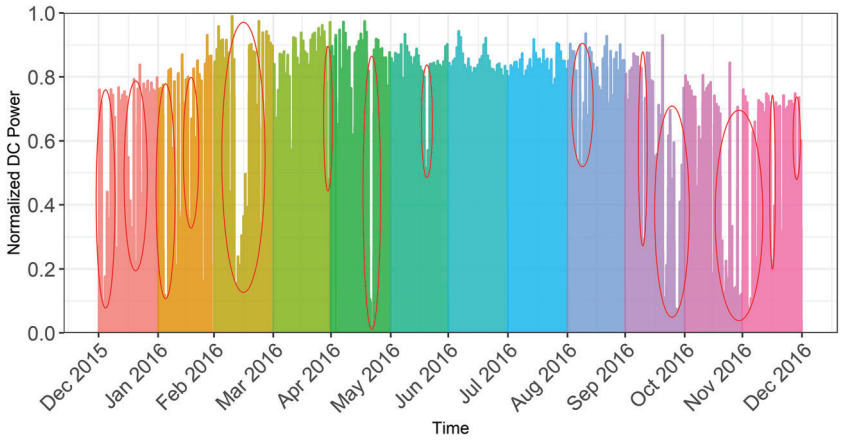

FIGURE 3 Profile of daily mean normalized DC power for inverter during a 1-year period. Examples of detected PV operational and data quality issues are circled in red

The four outcomes of the confusion matrix are defined as true positive (TP), true negative (TN), FP, and false negative (FN). The TN represents the fault data points that were correctly detected/classified, while the FN represents the normal operation data points that were incorrectly detected/classified as fault conditions. The TP represents the normal operation data points that were correctly detected/classified, while the FP represents the actual fault data points that were incorrectly detected/classified as normal operation points.[76] In this context, the accuracy metric is defined as the ratio of the number of correct predictions (TP + TN) to the number of total predictions (TP + TN + FP + FN).[75] The maintenance log of the system was used to verify actual normal and fault operation.

3 | RESULTS

The results correspond to data from one of the subsystems (Inverter 1) of the 1.8 MW plant.

3.1 | Data processing and quality verification application

The DQRs were applied to the PV dataset to filter out nighttime data points (i.e., G_I < 20 W/m^2). The power measurements were then normalized to the system's nominal capacity. The DQR process did not include data imputation nor correction to fully capture the exhibited profiles during fault conditions and loss events.

The DQRs methodology was also used to detect invalid measurements (that may indicate equipment malfunctions and/or faulty operation of the PV system) and to provide insights and information about possible failures/losses.[2] This was achieved by visually inspecting diagnostic plots, applying physical limits, statistical and comparative tests on the acquired measurements, and calculated PV performance parameters. Visual inspection of the Inverter 1 power data (see Figure 3) was deemed sufficient for observing PV operational problems (e.g., reduced power production) and data issues (e.g., gaps).[77]

3.2 | Normal PV system operation

Normal operation describes the expected operation of a well performing PV system without any fault conditions. During normal operating conditions, the PV system is affected only by environmental conditions and the measured power should be in good agreement with the predicted power (with a linear correlation coefficient higher than 0.9).[78] In such cases, no violations of the TL are detected, and the AE is below the set TL.

The measured and predicted DC power measurements of Inverter 1 over a 1-week period in August are depicted in Figure 4, demonstrating normal operation. Over the 1-week period in August, the DC power predictions of the Huld et al. model exhibited an R^2 of 0.99, while a MAPE of 8.6% and RMSE of 0.13 was obtained during the testing phase of the power predictive model. Although lower MAPE values have been reported in the literature for DC power predictions,[48] the model's validation process in such cases was performed either under normal operating conditions or on simulated data. In this paper, the model's performance was assessed using the 54 months test set, which contained both normal and fault conditions, and hence, higher MAPE values were obtained.

After evaluating the goodness of fit, a Shewhart chart[26,50] was constructed to verify the system's normal operation. As shown in Figure 5A, the power residuals were distributed within the estimated UCL and LCL during normal operation, while their mean was approximately zero. The residuals variance can be treated as a constant as shown in the histogram of the residuals (see Figure 5B). The histogram suggests that the residuals formulate approximately a normal distribution. Though, significant correlation in the residuals series was observed at different lags by the auto-correlation function (ACF) plot (Figure 5C), signifying the need for better seasonal adjustment.

3.3 | PV operation under fault and loss conditions

3.3.1 | Near zero power production incidents

During fault conditions, the measured DC power was significantly lower than the predicted and the comparative FDRs algorithm

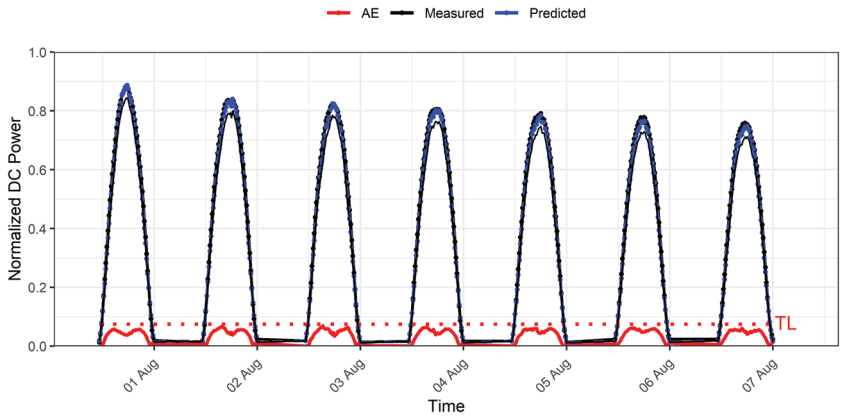

FIGURE 4 Normalized measured and predicted DC power of Inverter 1 for a 1-week period in August under normal operation. The absolute error (AE), defined as the absolute difference between the predicted and measured DC power, is represented by a red solid line. The set threshold level (TL) is indicated by a red dotted line

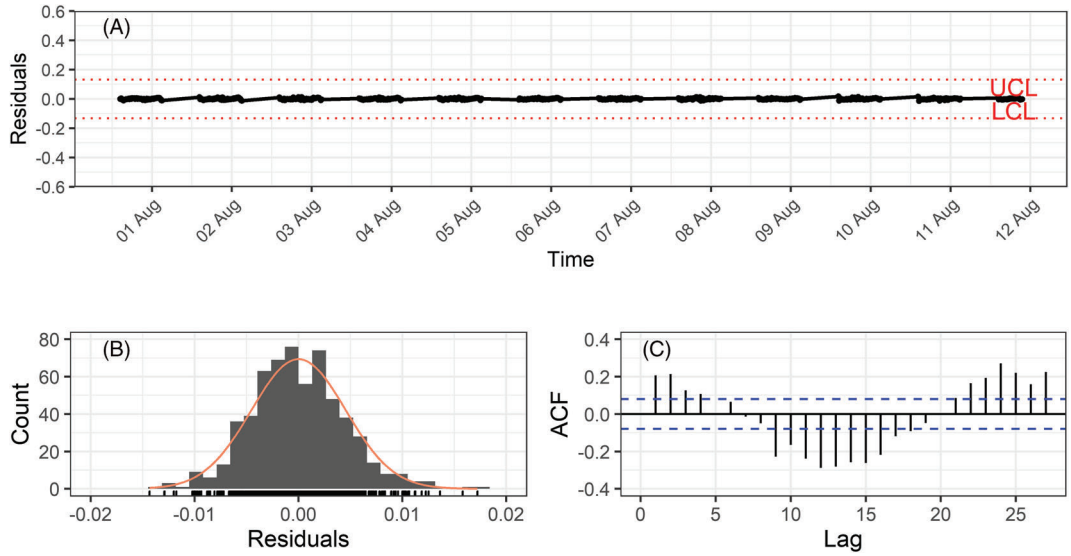

FIGURE 5 Normal operating conditions (A) normalized power residuals plot and imposed control limits by the three-sigma rule, (B) histogram of the normalized power residuals from the seasonal naïve method and normal curve colored in orange, and (C) auto-correlation function (ACF) plot

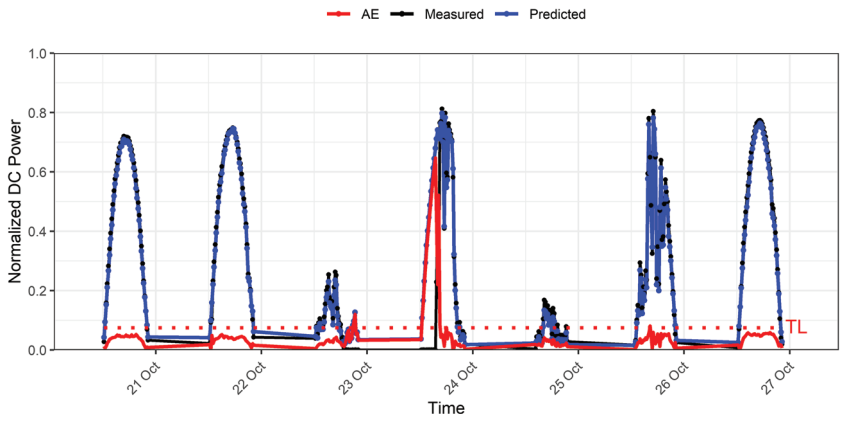

FIGURE 6 Normalized measured and predicted DC power of Inverter 1 for a 1-week period in October under normal operation and zero power production conditions. The absolute error (AE), defined as the absolute difference between the predicted and measured DC power, is colored in red solid line. The set threshold level (TL) is indicated by a red dotted line

detected several power discrepancies as the AE exceeded the set TL. During the test period, the failure detection stage detected 2229 data points (or 75 different days, during which fault incidents occurred) of near zero DC power production during daylight hours. The FDR detection stage achieved a detection accuracy of 97.3%, because from the 2229 detected data points, 1602, 567, 45, and 15 were classified as TP, TN, FN, and FP data points. The detected fault data points may be attributed to inverter shutdown failures, grid

failures, ground faults, and/or maintenance events. Communication and storage faults were excluded from this analysis. An example of a detected inverter failure (due to a ground fault) is shown in Figure 6 (see October 23 and 24). Information extracted from the maintenance log of the test PV plant indicated a failure incident that occurred on October 23 at 14:30 and was resolved on October 24 at 12:30.

Subsequently, the power residuals were analyzed using weekly sliding windows. As shown in Figure 7A, two data anomalies in the residuals pattern were detected in October indicating two fault occurrences. During the fault conditions, the residuals were not distributed within the estimated control limits and the mean of the residuals significantly deviated from zero for two specific cases (see October 20, 23, and 24). Furthermore, the residuals still formulate a normal distribution during the 2-week period as shown in Figure 7B, but they are spread out due to the larger standard deviation.

During near zero power production conditions, the affected parameters were mainly the DC power and current (reductions from 85% to 100%). The AC output power was also affected, and it was nearly zero. Such faults can affect either a part/subsystem or the whole PV system. Finally, the classification algorithm that considers the amount of power reduction, the affected electrical parameters, and the results of the statistical analysis achieved an accuracy of 97.3%. It is worth noting here that the classification stage achieved the same accuracy as the detection stage because this is a binary classification problem that involves classifying the data points into two groups: normal operation and fault data points.

3.3.2 | Nonzero power production due to fault occurrences – Reduced current class

The DC power time series of the test PV plant was subsequently examined for nonzero fault production incidents. An example of a detected nonzero fault production incident is shown in Figure 8. It can be seen that during the fault incident on October 20, the current (and hence the power) production was reduced by 49.3%. During that

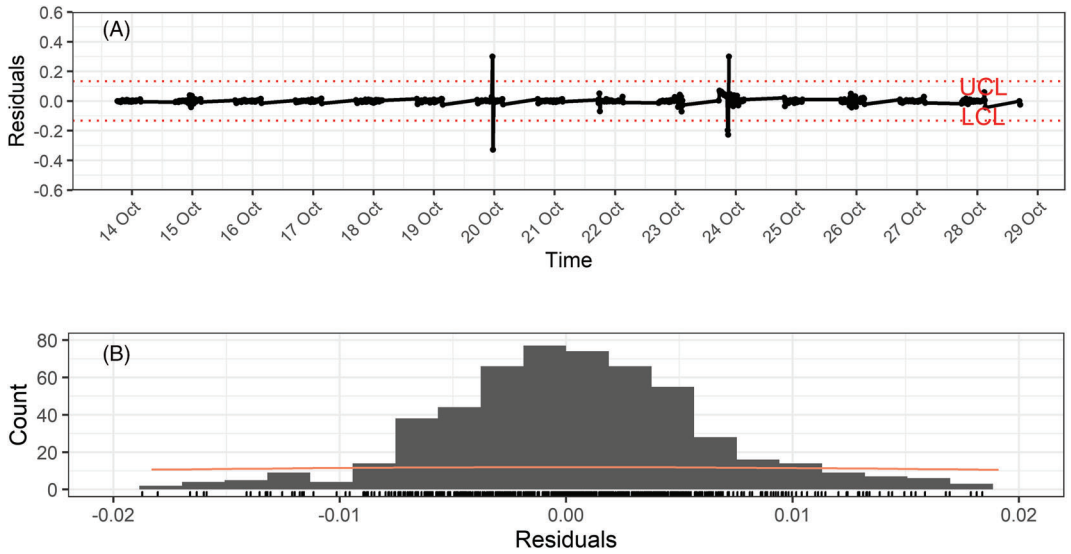

FIGURE 7 (A) Normalized power residuals plot and imposed control limits by the three-sigma rule and (B) histogram of the normalized power residuals from the seasonal naïve method during faulty operating conditions

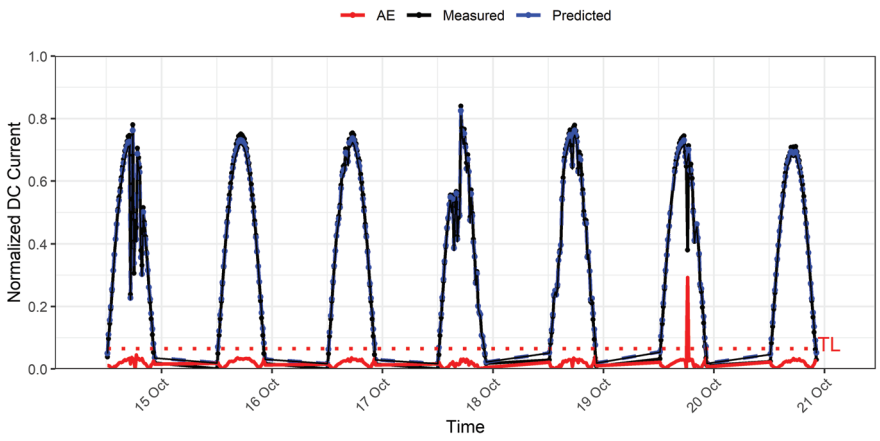

FIGURE 8 Normalized measured and predicted DC Current of Inverter 1 for a 1-week period under normal operation and nonzero power production conditions due to a fault occurrence (reduced current category). The absolute error (AE) is colored in red solid line. The set threshold level (TL) is indicated by a red dotted line

day, the voltage production remained within acceptable operating ranges, while the maintenance log of the test PV plant did not report any fault incidents.

As previously indicated in Figure 7A, a sudden change in the residual profile was detected on October 20, indicating a fault event. During that day, the current and power residuals exceeded the estimated control limits. Thus, the incident was classified as nonzero power production (reduction between 20% and 85%) due to "fault occurrences–reduced current class." Finally, the algorithm's classification accuracy could not be assessed because the maintenance log reported only fault issues at the inverter level.

3.3.3 | Nonzero power production incidents and categorization

The weekly PR time series (see Figure 9) was constructed using the recorded measurements of Inverter 1 over the period from June 2013 to December 2018. Visual inspection of PR in Figure 9 revealed a seasonal profile of the test subsystem, with higher PR values in the winter and lower in the summer. Additionally, low PR values were observed in December 2014–January 2015, January 2017, and June–August 2018. The S-H-ESD algorithm was initially applied to the PR time series and detected five data anomalies (circled in purple in Figure 9).

By correlating the PV system performance with the site's weather conditions, snowfall periods with low ambient temperature (<5°C) were detected during winter months, while heavy snowfall was reported by the data from MERRA-2[74] for the period covering December 2016–February 2017.

The FBP model was iteratively used to extract PLR and R_D. For PLR estimation, the FBP flexibility was set to 2.5 to capture a signal with all performance losses. Assuming linearity, no CP detection was performed, and linear regression with ordinary least squares (OLS) was directly applied on the FBP trend resulting in a PLR of −0.99%/year. The model's flexibility was then readjusted to 0.04 to extract the R_D by avoiding the influence of faults and temporary effects. The test subsystem demonstrated a linear power decline (see Figure 10), and by applying the OLS method to the linear extracted FBP trend (red color), a degradation rate of −0.49%/year was obtained. Even though PV degradation contributes to the PLR, the majority of the exhibited performance losses was found to be due to reversible and temporary phenomena.

The TLR methodology was then used for extracting soiling losses. Over the evaluation period, the FBP model detected 24 discontinuous CPs (i.e., cleaning events; indicated by red vertical lines in Figure 11)

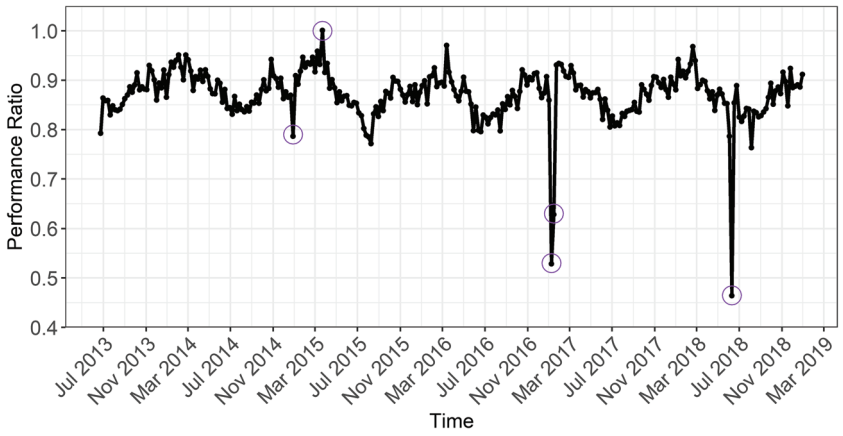

FIGURE 9 Weekly performance ratio (PR) time series of Inverter 1 over the evaluation period. Data anomalies detected by the Seasonal Hybrid Extreme Studentized Deviates (S-H-ESD) algorithm are circled in purple

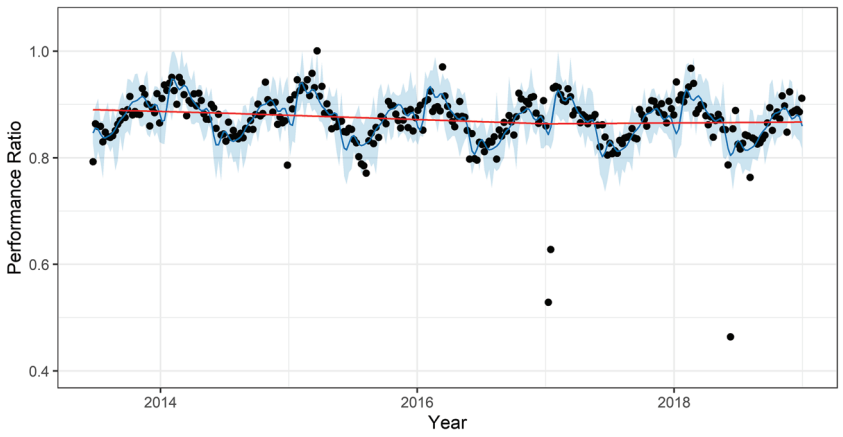

FIGURE 10 Weekly performance ratio (PR) time series (black dots) of the test PV system along with the extracted trend colored in red. The blue solid line is the Facebook Prophet (FBP) fit, while the blue shaded area indicates the uncertainty

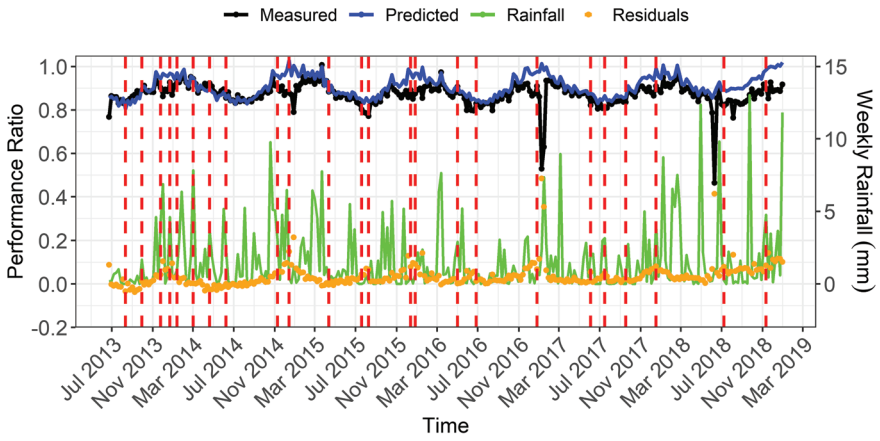

FIGURE 11 Weekly performance ratio (PR) time series (black line) and PR residuals (orange dots) of the test PV system. The predicted performance (blue line) of the system was simulated using the Huld et al.[46] model. The detected discontinuous change-points (CPs) by Facebook Prophet (FBP) are indicated with vertical lines. Green line: weekly rainfall, downloaded from MERRA-2. 74

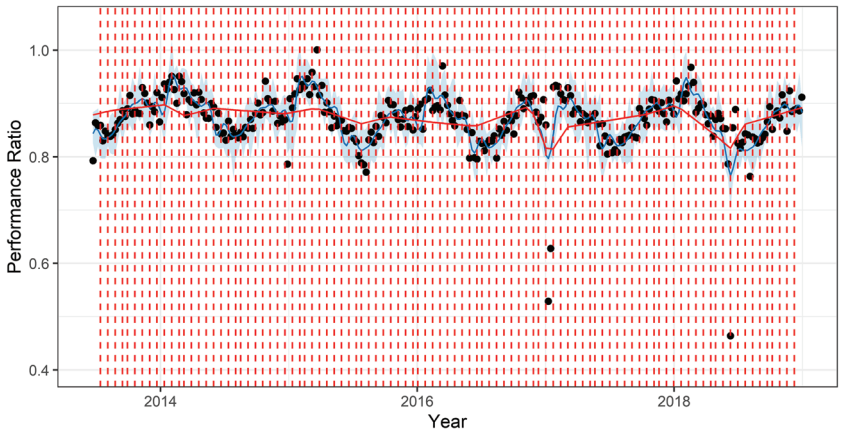

FIGURE 12 Weekly performance ratio (PR) time series (black dots) of the test PV system along with the distributed 100 potential change-points (CPs) colored in red dashed lines. The red solid line indicates the extracted trend, the blue solid line indicates the Facebook Prophet (FBP) fit, while the blue shaded area is the uncertainty

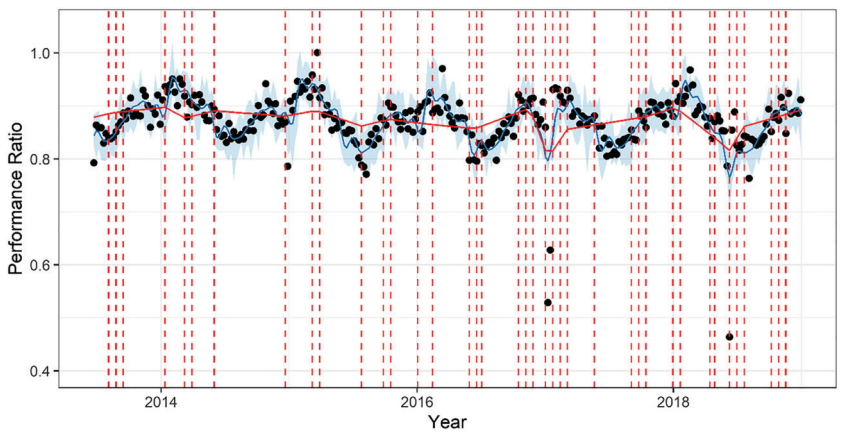

FIGURE 13 Weekly performance ratio (PR) time series (black dots) of the test PV system along with the 39 change-points (CPs) derived by the t test colored in red dashed lines. The red solid line indicates the extracted trend, the blue solid line indicates the Facebook Prophet (FBP) fit, while the blue shaded area is the uncertainty

in the residuals of the PR time series. Five of the cleaning events were reported in the maintenance log as periodic manual cleanings. Low to intermediate soiling losses were observed, with the soiling rates ranging from 0%/day to −0.69%/day.

Because there were indications of reversible (e.g., data anomalies in the PR time series, soiling) and irreversible (e.g., degradation) mechanisms, time series investigation for CPs detection was performed. The FBP algorithm was used to detect changes in the variability of the weekly PR time series and to differentiate the loss factors based on the CPs sequence and the corresponding rate of change. Initially, the FBP algorithm distributed 100 "potential" CPs uniformly along the PR time series trend (see Figure 12).

In order to derive the optimal number of CPs, the small sample hypothesis *t* test[79] was used. Based on the results of the statistical significance test, the critical threshold value for CPs was set to 0.0001 resulting in 39 CPs (see Figure 13). The FBP model also captured the data anomalies detected by S-H-ESD.

Different trend-based performance losses will exhibit different sequences (e.g., continuous or discontinuous CPs) and rates of change. For example, a heavy snowfall or a sandstorm will exhibit

steeper and faster rates of change compared with a change in degradation rate. In addition, because there are many locations in the time series where the rate can possibly change, most of the CPs remain unused due to the strength of the sparse prior defined by the *changepoint_prior_scale* hyperparameter of FBP. Therefore, the rates of change were examined to determine the most significant CPs and their causes. Positive rate changes (≥ 0) are due to artificial/manual cleaning events, snow shedding and PV system repairs. On the contrary, negative rates of change are due to fault occurrences and/or performance loss mechanisms.

In Figure 14, it can be seen that out of 39 CPs, 33 had nonzero rate of change. From those CPs, 12 had a positive rate of change, while 21 had a negative rate change. The FBP model then extracted the most significant CPs by considering the magnitude of the rate changes and at least 14 days between two consecutive CPs.[60] It is apparent from Figure 14 that 14 out of the 33 CPs had a minimal magnitude of rate change (i.e., below 0.2 in absolute values). From the remaining CPs, the two positive CPs detected in June 2016 and the two negative CPs in January 2018 occurred within a 2-week period.

FIGURE 14 Rate of change for the 39 change-points (CPs) detected by the Facebook Prophet (FBP) in the performance ratio (PR) time series. The rates of change represent differences in the slopes of the uniformly distributed CPs. CPs occur gradually; therefore, the peaks were selected to represent nonzero rate of change. From the 39 potential CPs, 33 had nonzero rate of change. Blue color indicates a positive rate change, while red color indicates a negative one

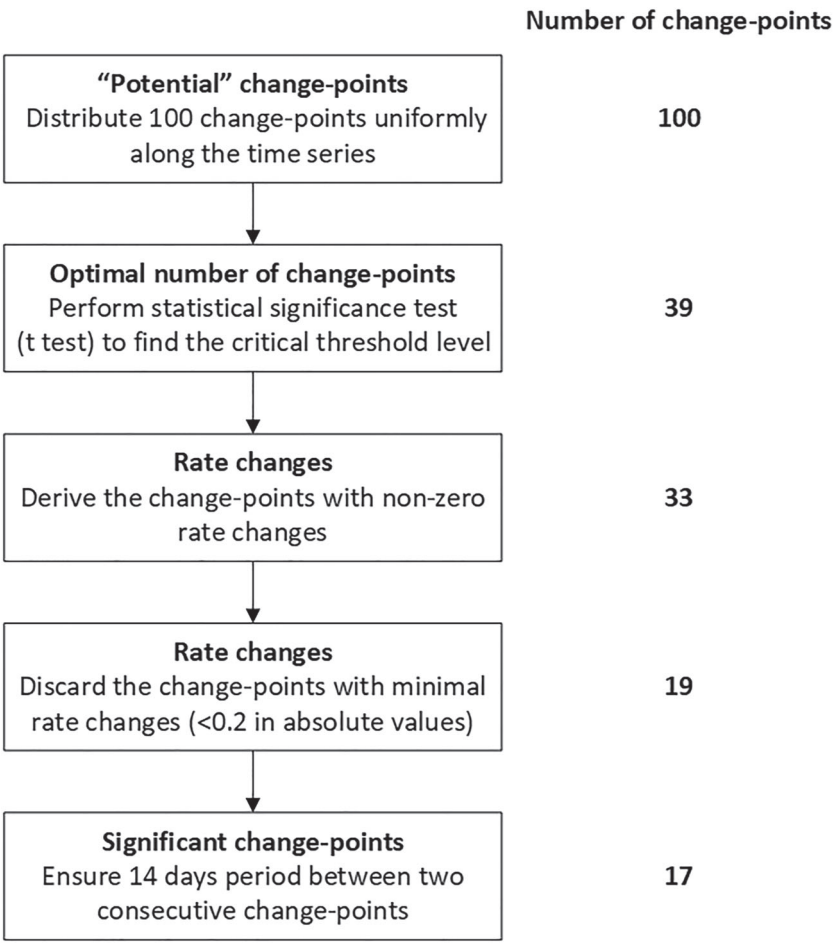

FIGURE 15 Exemplary flowchart depicting the procedure for extracting the significant change-points (CPs). The derived CPs at each step are also indicated

As such, FBP extracted 17 significant CPs (see Figure 15); 12 due to loss mechanisms and cleanings and 5 due to fault occurrences whereas 10 of them were negative (see Figure 16).

The rates of change were then coupled to weather data (e.g., see snowfall measurements indicated by green points in Figure 16) to determine the CP root cause. One significant CP was misclassified (the CP detected in December 2018), while the remaining 11 CPs were correctly distinguished as reversible loss mechanisms and differentiated from the five CPs due to faults (circled in purple in Figure 16). The TLR classification was verified against the maintenance log resulting in an accuracy of 91.66%. The CPs detected in December–January months (six detected in total, one misclassified) were attributed to snow coverage that caused gradual decrease of PV performance. From the remaining CPs due to loss and cleaning events, five were attributed to cleaning events, while one CP was due to soiling.

In cases of reversible trend-based performance losses, negative rate changes (<−0.2) are detected, while sharp positive changes (>0.2) are caused either by cleaning or snow shedding. Snow occurs during winter months with snowfall indications, and when the ambient temperature is "low" (<5°C [site/location-dependent value]). The PV performance is expected to increase when snow sheds. Similarly, soiling occurs during time periods with not enough rainfall, while the ambient temperature is >10°C (site/location-dependent value). After a cleaning event, an increase in PV performance is expected, while during soiling periods gradual reduction of PV performance is observed.

4 | EXHIBITED FAILURES AND PERFORMANCE LOSSES OF THE TEST PV PLANT

Over the evaluation period, the test subsystem produced 4068 MWh. The energy loss was then approximated as the difference between the predicted and measured DC energy yield resulting in 73.39 MWh (1.80%). The translation of the detected incidents into energy loss provides an indication of the magnitude of the economic loss for the PV plant owner. Because the test PV plant is currently monitored by an O&M company, the detected incidents were resolved based on the agreed response time, as stated in the contract made between the plant owner and the O&M company.[80] Therefore, the estimated energy loss represents the amount of lost energy generation during the period starting from the acknowledgment until the resolution time.[80]

Each category of energy loss is illustrated as a pie chart in Figure 17. Most of the energy loss was attributed to near zero power production incidents by 43.40% (e.g., inverter faults), while nonzero production incidents accounted for 42.87% (e.g., reduced current

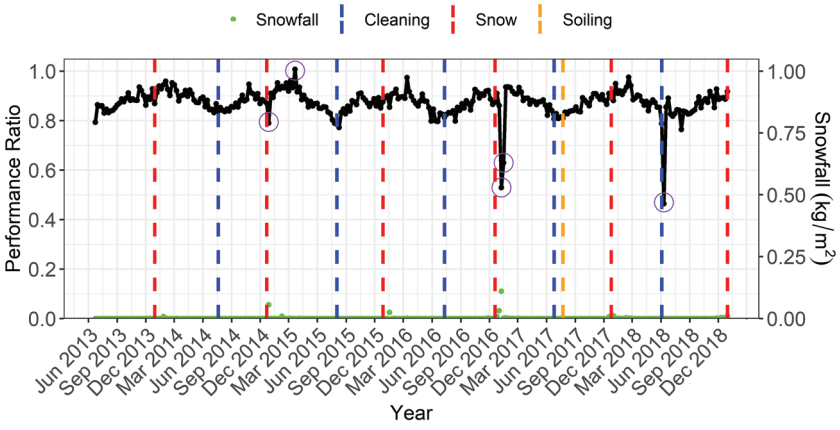

FIGURE 16 Weekly performance ratio (PR) time series (black dots) of the test PV system along with the detected significant change-points (CPs) indicated by dashed lines. The red dashed lines indicate snow events, the blue dashed lines indicate cleaning events, and the orange line indicates soiling. Data anomalies detected by the Seasonal Hybrid Extreme Studentized Deviates (S-H-ESD) algorithm are circled in purple including heavy snowfalls. Weekly snowfall measurements are indicated by green points

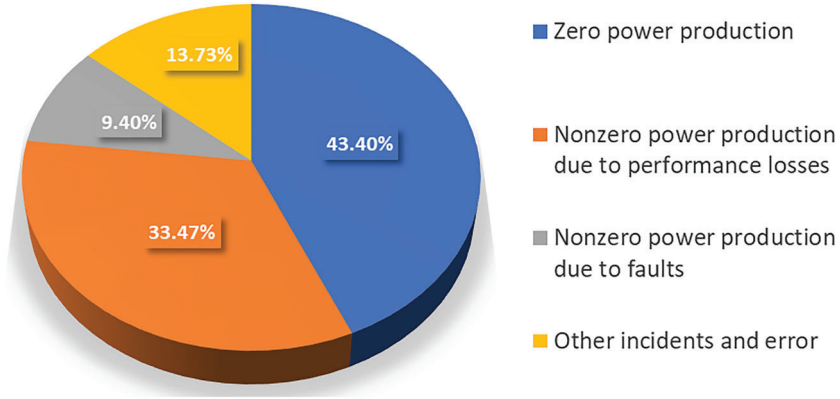

FIGURE 17 Pie chart depicting the faction of the total energy lost in the test subsystem due to different fault and loss incidents

production), from which 33.47% was due to performance losses (soiling, degradation, and snow). Finally, a 13.73% was attributed to other incidents and the power model's error.

The proposed diagnostic architecture suffers from the following limitations: (a) the CP model's flexibility needs to be recalibrated depending on the application and when using different performance metrics and (b) the methodology for extracting the significant number of CPs is not fully automated. Furthermore, given the available field data, the "actual" loss of energy generation for the test subsystem could not be estimated; only the energy lost during the period starting from the acknowledgment time until the resolution time was estimated. Despite the limitations of the proposed methodology, this is the first attempt in differentiating faults from reversible and irreversible performance losses using a statistical approach and a single performance metric. Based on the results from the analysis of such field data, O&M teams can be informed about the underperformance issues and act accordingly in order to recover some of the performance and financial losses.

5 | CONCLUSIONS

An analytical architecture capable of detecting underperformance issues in PV systems due to failures and loss mechanisms was presented in this work. The proposed architecture operates entirely on acquired raw field measurements. It mainly focuses on differentiating commonly exhibited failures from trend-based performance losses using a single performance metric.

The developed pipeline was experimentally validated using historical inverter data obtained from a large-scale PV system installed in Greece. The results demonstrated the effectiveness of the routines for detecting failures and loss mechanisms and the capability of the pipeline for distinguishing underperformance issues using residual, anomaly detection, and CP techniques. A CP model, namely, the FBP, was also used to extract significant changes in time series data, to detect soiling cleaning events and to estimate both reversible and irreversible performance losses in PV systems.

Finally, only inverter data were available in this study, and differentiation of faults from loss factors was performed at the inverter level. Future work will be extending the fault and loss categories and include more root causes such as partial shading, vegetation, and PV module-level failures which, in turn, require string/module-level monitoring. The results from the application of the proposed diagnostic pipeline can be used for monitoring applications and for optimizing O&M activities.

ACKNOWLEDGEMENTS

The work of the Andreas Livera, Leonardo Micheli, and George E. Georghiou was supported by the ROM-PV project under the umbrella of SOLAR-ERA.NET Cofund by the General Secretariat for Research and Technology (GSRT), the Ministry of Economy, Industry and Competitiveness—State Research Agency (MINECO-AEI), and the Research and Innovation Foundation (RIF) of Cyprus. SOLAR-ERA.NET is supported by the European Commission within the EU Framework Programme for Research and Innovation HORIZON 2020 (Cofund ERA-NET Action, No. 691664).

The work of Marios Theristis and Joshua S. Stein was supported by the U.S. Department of Energy's Office of Energy Efficiency and Renewable Energy (EERE) under the Solar Energy Technologies Office Award Number 38267. Sandia National Laboratories is a multimission laboratory managed and operated by National Technology & Engineering Solutions of Sandia, LLC, a wholly owned subsidiary of Honeywell International Inc., for the U.S. Department of Energy's National Nuclear Security Administration under contract DE-NA0003525. This article describes objective technical results and analysis. Any subjective views or opinions that might be expressed in this article do not necessarily represent the views of the U.S. Department of Energy or the Unites States Government.

Alectris Hellas IKE is kindly acknowledged for providing the field data of the test PV plant.

CONFLICT OF INTEREST

The author declares that there is no conflict of interest that could be perceived as prejudicing the impartiality of the research reported.

DATA AVAILABILITY STATEMENT

The data that support the findings of this study are available from ALECTRIS HELLAS IKE. Restrictions apply to the availability of these data, which were used under license for this study. Data are available from the author(s) with the permission of ALECTRIS HELLAS IKE.

ORCID

Andreas Livera https://orcid.org/0000-0002-3732-9171
Marios Theristis https://orcid.org/0000-0002-7265-4922
Leonardo Micheli https://orcid.org/0000-0001-7986-7560
Joshua S. Stein https://orcid.org/0000-0002-9422-1976
George E. Georghiou https://orcid.org/0000-0002-5872-5851

REFERENCES

1. European Technology and Innovation Platform for Photovoltaics (ETIP PV). *Photovoltaic Solar Energy: Big and Beyond Sustainable Energy to Limit Global Warming to 1.5 Degrees*. Secretariat of the ETIP PV; 2019.
2. Livera A, Theristis M, Charalambous A, Stein JS, Georghiou GE. Decision support system for corrective maintenance in large-scale photovoltaic systems. In: *48th IEEE Photovoltaic Specialist Conference (PVSC)*. IEEE; 2021:0306-0311. doi:10.1109/PVSC43889.2021.9518796.
3. Livera A, Theristis M, Makrides G, Georghiou GE. Recent advances in failure diagnosis techniques based on performance data analysis for grid-connected photovoltaic systems. *Renew Energy*. 2019;133:126-143. doi:10.1016/j.renene.2018.09.101
4. Livera A, Theristis M, Koumpli E, et al. Data processing and quality verification for improved photovoltaic performance and reliability analytics. *Prog Photovoltaics Res Appl*. 2021;29(2):143-158. doi:10.1002/pip.3349
5. Caputo D, Grimaccia F, Mussetta M, Zich RE. Photovoltaic plants predictive model by means of ANN trained by a hybrid evolutionary

algorithm. In: *The 2010 International Joint Conference on Neural Networks (IJCNN)*. IEEE; 2010:1-6.
6. Kalogirou SA. Applications of artificial neural-networks for energy systems. *Appl Energy*. 2000;67(1-2):17-35. doi:10.1016/S0306-2619(00)00005-2
7. Cheng Z, Zhong D, Li B, Liu Y. Research on fault detection of PV array based on data fusion and fuzzy mathematics. In: *2011 Asia-Pacific Power and Energy Engineering Conference*. IEEE; 2011.
8. Sun J, Sun F, Fan J, Liang Y. Fault diagnosis model of photovoltaic array based on least squares support vector machine in Bayesian framework. *Appl Sci*. 2017;7(11):1199. doi:10.3390/app7111199
9. Zuniga-Reyes MA, Robles-Ocampo JB, Sevilla-Camacho PY, Rodriguez-Resendiz J, Lastres-Danguillecourt O, Conde-Diaz JE. Photovoltaic failure detection based on string-inverter voltage and current signals. *IEEE Access*. 2021;9:39939-39954. doi:10.1109/ACCESS.2021.3061354
10. Zhao Y, Yang L, Lehman B, de Palma JF, Mosesian J, Lyons R. Decision tree-based fault detection and classification in solar photovoltaic arrays. In: *2012 Twenty-Seventh Annual IEEE Applied Power Electronics Conference and Exposition (APEC)*. IEEE; 2012:93-99. doi:10.1109/APEC.2012.6165803.
11. Tsanakas JA, Chrysostomou D, Botsaris PN, Gasteratos A. Fault diagnosis of photovoltaic modules through image processing and Canny edge detection on field thermographic measurements. *Int J Sustain Energy*. 2015;34(6):351-372. doi:10.1080/14786451.2013.826223
12. Mekki H, Mellit A, Salhi H. Artificial neural network-based modelling and fault detection of partial shaded photovoltaic modules. *Simul Model Pract Theory*. 2016;67:1-13. doi:10.1016/j.simpat.2016.05.005
13. Dhimish M, Holmes V, Mehrdadi B, Dales M. Comparing Mamdani Sugeno fuzzy logic and RBF ANN network for PV fault detection. *Renew Energy*. 2018;117:257-274. doi:10.1016/j.renene.2017.10.066
14. Samara S, Natsheh E. Intelligent real-time photovoltaic panel monitoring system using artificial neural networks. *IEEE Access*. 2019;7:50287-50299. doi:10.1109/ACCESS.2019.2911250
15. Fazai R, Abodayeh K, Mansouri M, et al. Machine learning-based statistical testing hypothesis for fault detection in photovoltaic systems. *Sol Energy*. 2019;190(August):405-413. doi:10.1016/j.solener.2019.08.032
16. Kumar S, Selvakumar A. Detection of the faults in the photovoltaic array under normal and partial shading conditions. In: *International Conference on Innovations in Power and Advanced Computing Technologies*. IEEE; 2017:1-5.
17. Belaout A, Krim F, Mellit A, Talbi B, Arabi A. Multiclass adaptive neuro-fuzzy classifier and feature selection techniques for photovoltaic array fault detection and classification. *Renew Energy*. 2018;127:548-558. doi:10.1016/j.renene.2018.05.008
18. Ducange P, Fazzolari M, Lazzerini B, Marcelloni F. An intelligent system for detecting faults in photovoltaic fields. In: *11th International Conference on Intelligent Systems Design and Applications (ISDA)*. IEEE; 2011:1341-1346. doi:10.1109/ISDA.2011.6121846.
19. Dhimish M, Holmes V, Mehrdadi B, Dales M. Diagnostic method for photovoltaic systems based on six layer detection algorithm. *Electr Pow Syst Res*. 2017;151:26-39. doi:10.1016/j.epsr.2017.05.024
20. Platon R, Martel J, Woodruff N, Chau TY. Online fault detection in PV systems. *IEEE Trans Sustain Energy*. 2015;6(4):1200-1207. doi:10.1109/TSTE.2015.2421447
21. Platon R, Pelland S, Poissant Y. Modelling the power production of a photovoltaic system: comparison of sugeno-type fuzzy logic and PVSAT-2 models. In: EuroSun 2012 - *Europe Solar Conference (ISES)*; 2012.
22. Zhao Y, Lehman B, Ball R, Mosesian J, De Palma J-F. Outlier detection rules for fault detection in solar photovoltaic arrays. In: *2013 28th Annual IEEE Applied Power Electronics Conference and Exposition (APEC)*. IEEE; 2013:2913-2920.
23. Stettler S, Toggweiler P, Wiemken E, et al. Failure detection routine for grid connected PV systems as part of the PVSAT-2 project. In: *20th European Photovoltaic Solar Energy Conference*; 2005.
24. Drews A, de Keizer AC, Beyer HG, et al. Monitoring and remote failure detection of grid-connected PV systems based on satellite observations. *Sol Energy*. 2007;81(4):548-564. doi:10.1016/j.solener.2006.06.019
25. Garoudja E, Harrou F, Sun Y, Kara K, Chouder A, Silvestre S. Statistical fault detection in photovoltaic systems. *Sol Energy*. 2017;150:485-499. doi:10.1016/j.solener.2017.04.043
26. Harrou F, Sun Y, Taghezouit B, Saidi A, Hamlati ME. Reliable fault detection and diagnosis of photovoltaic systems based on statistical monitoring approaches. *Renew Energy*. 2018;116:22-37. doi:10.1016/j.renene.2017.09.048
27. Phinikarides A, Makrides G, Kindyni N, Georghiou GE. Comparison of trend extraction methods for calculating performance loss rates of different photovoltaic technologies. In: *2014 IEEE 40th Photovoltaic Specialist Conference (PVSC)*. IEEE; 2014:3211-3215. doi:10.1109/PVSC.2014.6925619.
28. Chouder A, Silvestre S. Automatic supervision and fault detection of PV systems based on power losses analysis. *Energ Conver Manage*. 2010;51(10):1929-1937. doi:10.1016/j.enconman.2010.02.025
29. Chao KH, Ho SH, Wang MH. Modeling and fault diagnosis of a photovoltaic system. *Electr Pow Syst Res*. 2006;78(1):97-105. doi:10.1016/j.epsr.2006.12.012
30. Jones CB, Theristis M, Stein JS, Hansen C. Feature selection of photovoltaic system data to avoid misclassification of fault conditions. In: *2020 47th IEEE Photovoltaic Specialists Conference (PVSC)*. IEEE; 2020:1357-1362. doi:10.1109/PVSC45281.2020.9300786.
31. Morente-Molinera JA, Mezei J, Carlsson C, Herrera-Viedma E. Improving supervised learning classification methods using multigranular linguistic modeling and fuzzy entropy. *IEEE Trans Fuzzy Syst*. 2017;25(5):1078-1089. doi:10.1109/TFUZZ.2016.2594275
32. Akram MN, Lotfifard S. Modeling and health monitoring of DC side of photovoltaic array. *IEEE Trans Sustain Energy*. 2015;6(4):1245-1253. doi:10.1109/TSTE.2015.2425791
33. Livera A, Makrides G, Sutterlueti J, Georghiou GE. Advanced failure detection algorithms and performance decision classification for grid-connected PV systems. In: *33rd European Photovoltaic Solar Energy Conference and Exhibition (EU PVSEC)*; 2017:2358-2363. doi:10.4229/EUPVSEC20172017-6BV.2.13.
34. Zhao Y, Ball R, Mosesian J, de Palma J-F, Lehman B. Graph-based semi-supervised learning for fault detection and classification in solar photovoltaic arrays. *IEEE Trans Power Electron*. 2015;30(5):2848-2858. doi:10.1109/TPEL.2014.2364203
35. Massi Pavan A, Mellit A, De Pieri D, Kalogirou SA. A comparison between BNN and regression polynomial methods for the evaluation of the effect of soiling in large scale photovoltaic plants. *Appl Energy*. 2013;108:392-401. doi:10.1016/j.apenergy.2013.03.023
36. Chen Z, Wu L, Cheng S, Lin P, Wu Y, Lin W. Intelligent fault diagnosis of photovoltaic arrays based on optimized kernel extreme learning machine and I-V characteristics. *Appl Energy*. 2017;204:912-931. doi:10.1016/j.apenergy.2017.05.034
37. Wu Y, Chen Z, Wu L, Lin P, Cheng S, Lu P. An intelligent fault diagnosis approach for PV array based on SA-RBF kernel extreme learning machine. *Energy Procedia*. 2017;105:1070-1076. doi:10.1016/j.egypro.2017.03.462
38. Lin P, Lin Y, Chen Z, Wu L, Chen L, Cheng S. A density peak-based clustering approach for fault diagnosis of photovoltaic arrays. *Int J Photoenergy*. 2017;2017:4903613. https://www.hindawi.com/journals/ijp/2017/4903613/abs/

39. Li L, Ding SX, Yang Y, Peng K, Qiu J. A fault detection approach for nonlinear systems based on data-driven realizations of fuzzy kernel representations. *IEEE Trans Fuzzy Syst*. 2018;26(4):1800-1812. doi:10.1109/TFUZZ.2017.2752136
40. Holmgren FW, Hansen WC, Mikofski AM. pvlib python: a python package for modeling solar energy systems. *J Open Source Softw*. 2018;3(29):884. doi:10.21105/joss.00884
41. Jordan DC, Deline C, Kurtz SR, Kimball GM, Anderson M. Robust PV degradation methodology and application. *IEEE J Photovoltaics*. 2018; 8(2):525-531. doi:10.1109/JPHOTOV.2017.2779779
42. Deceglie MG, Jordan D, Shinn A, Deline C. *Rdtools: An Open Source Python Library for PV Degradation Analysis Degradation Rate*. In: 2018 PV Systems Symposium; 2018:1-15. Available at: https://www.osti.gov/servlets/purl/1436856
43. Skomedal A, Deceglie MG. Combined estimation of degradation and soiling losses in photovoltaic systems. *IEEE J Photovoltaics*. 2020; 10(6):1788-1796. doi:10.1109/JPHOTOV.2020.3018219
44. Lantz B. *Machine learning with R*. Packt Publishing Ltd; 2013. doi:10.1007/978-981-10-6808-9.
45. Ray S, McEvoy DS, Aaron S, Hickman TT, Wright A. Using statistical anomaly detection models to find clinical decision support malfunctions. *J Am Med Inform Assoc*. 2018;25(7):862-871. doi:10.1093/jamia/ocy041
46. Huld T, Friesen G, Skoczek A, et al. A power-rating model for crystalline silicon PV modules. *Sol Energy Mater Sol Cells*. 2011;95(12):3359-3369. doi:10.1016/j.solmat.2011.07.026
47. Koumpli E. *Impact of Data Quality on Photovoltaic (PV) Performance Assessment*, Doctoral Thesis. University of Loughborough; 2017.
48. Livera A, Theristis M, Makrides G, Sutterlueti J, Ransome S, Georghiou GE. Performance analysis of mechanistic and machine learning models for photovoltaic energy yield prediction. In: *36th European Photovoltaic Solar Energy Conference (EU PVSEC)*; 2019: 1272-1277. doi:10.4229/EUPVSEC20192019-5BO.5.2.
49. Makrides G, Zinsser B, Schubert M, Georghiou GE. Energy yield prediction errors and uncertainties of different photovoltaic models. *Prog Photovoltaics Res Appl*. 2013;21:500-516. doi:10.1002/pip.1218
50. Hart MK, Hart RF. Shewhart control charts for individuals with time-ordered data. *Front Stat Qual Control*. 1992;4:123-137. doi:10.1007/978-3-662-11789-7_9
51. Branco P, Gonçalves F, Costa AC. Tailored algorithms for anomaly detection in photovoltaic systems. *Energies*. 2020;13(1):225. doi:10.3390/en13010225
52. King DL, Boyson WE, Kratochvill JA. *Photovoltaic Array Performance Model, SANDIA Report SAND2004-3535*. Vol. 8. Sandia National Laboratories (SNL); 2004. doi:10.2172/919131.
53. Ross RG. Interface design considerations for terrestrial solar cell modules. In: *12th IEEE Photovoltaic Specialist Conference (PVSC)*. IEEE; 1976:801-806. https://ui.adsabs.harvard.edu/abs/1976pvsp.conf..801R
54. Anadol MA, Erhan E. The effect of snowfall and icing on the sustainability of the power output of a grid-connected photovoltaic system in Konya, Turkey. *Turkish J Electr Eng Comput Sci*. 2019;27(6):4608-4623. doi:10.3906/ELK-1901-178
55. Huang J, Li H, Sun Y, Wang H, Yang H. Investigation on potential-induced degradation in a 50MWp crystalline silicon photovoltaic power plant. *Int J Photoenergy*. 2018;2018:3286124. doi:10.1155/2018/3286124
56. Jordan DC, Kurtz SR. Photovoltaic degradation rates—an analytical review. *Prog Photovoltaics Res Appl*. 2013;21(1):12-29. doi:10.1002/pip.1182
57. Kaaya I, Lindig S, Weiss KA, et al. Photovoltaic lifetime forecast model based on degradation patterns. *Prog Photovoltaics Res Appl*. 2020; 28(10):979-992. doi:10.1002/pip.3280
58. Theristis M, Livera A, Jones CB, Makrides G, Georghiou GE, Stein JS. Nonlinear photovoltaic degradation rates: modeling and comparison against conventional methods. *IEEE J Photovoltaics*. 2020;10(4):1112-1118. doi:10.1109/JPHOTOV.2020.2992432
59. Theristis M, Livera A, Micheli L, et al. Modeling nonlinear photovoltaic degradation rates. In: *47th IEEE Photovoltaic Specialist Conference (PVSC)*. IEEE; 2020:0208-0212. doi:10.1109/PVSC45281.2020.9300388.
60. Micheli L, Theristis M, Livera A, et al. Improved PV soiling extraction through the detection of cleanings and change points. *IEEE J Photovoltaics*. 11(2):519-526. doi:10.1109/JPHOTOV.2020.3043104
61. Romero-Fiances I, Livera A, Theristis M, et al. Impact of duration and missing data on the long-term photovoltaic degradation rate estimation. *Renew Energy*. 2021;181:738-748. doi:10.1016/j.renene.2021.09.078
62. Taylor SJ, Letham B. Forecasting at scale. *Peer J Preprints*. 2017;35(8): 48-90. doi:10.7287/peerj.preprints.3190v2
63. Holt CC. Forecasting seasonals and trends by exponentially weighted moving averages. *Int J Forecast*. 2004;20(1):5-10. doi:10.1016/j.ijforecast.2003.09.015
64. Theristis M, Livera A, Micheli L, et al. Comparative analysis of change-point techniques for nonlinear photovoltaic performance degradation rate estimations. *IEEE J Photovoltaics*. 2021;11(6):1511-1518. doi:10.1109/JPHOTOV.2021.3112037
65. Taylor S, Letham B. *Automatic Forecasting Procedure—Package 'Prophet'*. 2021. https://github.com/facebook/prophet
66. Skomedal Å, Haug H, Marstein ES. Endogenous soiling rate determination and detection of cleaning events in utility-scale PV plants. *IEEE J Photovoltaics*. 2019;9(3):858-863. doi:10.1109/JPHOTOV.2019.2899741
67. Rosner B. Percentage points for a generalized ESD many-outlier procedure. *Dent Tech*. 1983;25(2):165-172. doi:10.1080/00401706.1983.10487848
68. Rosner B. On the detection of many outliers. *Dent Tech*. 1975;17(2): 221-227.
69. Twitter. *AnomalyDetection R package*. https://github.com/twitter/AnomalyDetection. 2015.
70. Øgaard MB, Aarseth BL, Skomedal ÅF, Riise HN, Sartori S, Selj JH. Identifying snow in photovoltaic monitoring data for improved snow loss modeling and snow detection. *Sol Energy*. 2021;223(May):238-247. doi:10.1016/j.solener.2021.05.023
71. Ascencio-Vásquez J, Brecl K, Topič M. Methodology of Köppen-Geiger-Photovoltaic climate classification and implications to worldwide mapping of PV system performance. *Sol Energy*. 2019; 191(August):672-685. doi:10.1016/j.solener.2019.08.072
72. International Electrotechnical Commission. *IEC 61724-1:2017. Photovoltaic System Performance—Part 1: Monitoring*. IEC; 2017.
73. Theristis M, Venizelou V, Makrides G, Georghiou GE. Chapter II-1-B—energy yield in photovoltaic systems. In: Kalogirou SA, ed. *McEvoy's Handbook of Photovoltaics*. 3rd ed. Academic Press; 2018:671-713.
74. Global Modeling and Assimilation Office (GMAO). *MERRA-2 tavg1_2d_slv_Nx: 2d, 1-Hourly, Time-Averaged, Single-Level, Assimilation, Single-Level Diagnostics V5.12.4*. Greenbelt, MD, USA: Goddard Earth Sciences Data and Information Services Center (GES DISC); 2015. doi:10.5067/VJAFPLI1CSIV.
75. Dhimish M, Holmes V, Mehrdadi B, Dales M, Mather P. Photovoltaic fault detection algorithm based on theoretical curves modelling and fuzzy classification system. *Energy*. 2017;140:276-290. doi:10.1016/j.energy.2017.08.102
76. Livera A, Theristis M, Makrides G, Georghiou GE. On-line failure diagnosis of grid-connected photovoltaic systems based on fuzzy logic. In: *12th IEEE International Conference on Compatibility, Power Electronics*

and Power Engineering (CPE-POWERENG). IEEE; 2018. doi:10.1109/CPE.2018.8372537.

77. Lindig S, Louwen A, Moser D, Topic M. Outdoor PV system monitoring—input data quality, data imputation and filtering approaches. *Energies*. 2020;13:5099. doi:10.3390/enxx010005
78. Building Research Establishmen (BRE). *Domestic Photovoltaic Field Trials—Final Technical Report*. Building Research Establishment, Watford, UK; 2006.
79. Saylor Academy. Introductory Statistics. v. 1. Saylor Academy. 2012. https://saylordotorg.github.io/text_introductory-statistics/index.html
80. SolarPower Europe (SPE). *Operation & Maintenance Best Practice Guidelines/Version 4.0*. SPE; 2019.

How to cite this article: Livera A, Theristis M, Micheli L, Stein JS, Georghiou GE. Failure diagnosis and trend-based performance losses routines for the detection and classification of incidents in large-scale photovoltaic systems. *Prog Photovolt Res Appl*. 2022;1-17. doi:10.1002/pip.3578